International Journal of Heat and Mass Transfer 183 (2022) 122238

Contents lists available at ScienceDirect

International Journal of Heat and Mass Transfer

journal homepage: www.elsevier.com/locate/hmt

Verification of the method of reconstructing convective velocity fields on the basis of temperature fields in vertical, differential and equally heated, open and closed channels

Krzysztof Tesch [a], Michał Ryms [b,b,*], Witold M. Lewandowski [b]

[a] Faculty of Mechanical Engineering and Ship Technology, Institute of Energy, Gdańsk University of Technology, Narutowicza 11/12, Gdańsk 80-233, Poland
[b] Faculty of Chemistry, Department of Energy Conversion and Storage, Gdańsk University of Technology, Narutowicza 11/12, Gdańsk 80-233, Poland

ARTICLE INFO

Article history:
Received 8 September 2021
Revised 27 October 2021
Accepted 7 November 2021
Available online 17 November 2021

Keywords:
Free convection
Differentially and equally heated channel
Numerical velocity field reconstruction
Temperature field detection
Infrared imaging
CFD

ABSTRACT

This paper describes a method of reconstructing velocity fields, i.e. a numerical reconstruction procedure (NRP) that involves the numerical processing of experimentally measured temperature distributions in free convection heat transfer. The NRP consists in solving only the continuity and Navier–Stokes equations with an additional source term. This term is proportional to a known temperature (e.g. from a thermal imaging camera) and replaces the Fourier–Kirchhoff equation, which also means that the NRP does not require boundary conditions associated with the temperature to be formulated.

In order to verify the NRP, the experimental results of two published cases were taken into consideration. In the first case, the temperature and velocity distributions were determined during free convection heat transfer in a closed cavity, i.e. in a vertical channel formed between differentially heated plates. Subsequently, the velocity distributions obtained by the NRP were compared directly with the experimental results. However, in order to verify the correctness of this method for the entire field, not just for the individual locations, free convection heat transfer measurements in an open channel formed between two isothermal, equally heated plates were considered. A thermal imaging camera was used to detect the temperature field in air. In this case, verification of the NRP method required the results obtained in the form of a reconstructed velocity field to be compared with a field obtained using standard numerical calculations (SNC).

Importantly, the NRP provides new opportunities for thermal imaging cameras equipped with a mesh for air temperature detection, for example, the visualisation of air velocity fields in free convective heat transfer.

1. Introduction

The description of heat transfer by free convection, especially in the case of low temperatures of the heating surface, small temperature differences and gradients, and minimum heating powers, is a rather difficult research problem, not only theoretically, but also, or even mainly, experimentally. Accurate, simultaneous measurements of temperature and velocity, or the determination of heat fluxes on their basis, are relatively difficult to perform owing to the very small but constantly changing temperatures (fluctuations) in moving convective streams.

Such problems may be encountered when analysing the free convection from any heating surface in a channel formed by two vertical walls, especially in more complex configurations and geometric variants, where access to the individual parts of the installation may be very difficult. Unfortunately, one comes across such cases quite often nowadays, for example, in heating technology (radiators), construction and electronics, energy and many other technical solutions. In this situation, there is increasing support for applying numerical modelling to some cases of convective heat transfer, especially the more difficult ones [7,15,31]. However, this often requires time-consuming work on each problem separately, and even then there is no absolute certainty whether such a

Abbreviations: CTM, camera temperature measurements; NRP, numerical reconstruction procedure; SNC, standard numerical calculation.

* corresponding author.
E-mail address: michal.ryms@pg.edu.pl (M. Ryms).

https://doi.org/10.1016/j.ijheatmasstransfer.2021.122238

Nomenclature

A	width
B	channel thickness
Co	Courant number
c_p	specific heat capacity
f	index number of planar surfaces S_f around a control volume V_P
$\mathbf{g}$, g	gravity acceleration vector, magnitude of $\mathbf{g}$
H	channel height
k	turbulence kinetic energy
p, p_k	pressure, kinematic pressure
P	centroid of a finite volume V_P
Pr, $\mathrm{Pr_t}$	Prandtl and turbulent Prandtl numbers
$\mathbf{r}$	position vector
Ra	Rayleigh number
S	channel width
S_f	planar surface
$\mathbf{S}_f$	surface normal vector pointing outward
$\mathbf{S}_u$	explicit momentum source
t	time
T	temperature
$\mathbf{u}$	velocity vector field
u_x, u_y	velocity components
$\lvert V_P \rvert$	control volume measure around a centroid P
x, y, z	Cartesian coordinates
β	coefficient of volumetric expansion
μ	dynamic viscosity
ν	kinematic viscosity
ν_t	eddy viscosity
ρ	density
ω	turbulence frequency (specific dissipation rate)

numerically solved case actually reflects reality. In addition, there is no substitute for direct measurement, without which one cannot verify either theoretical solutions or numerical calculations. In convection studies, therefore, in parallel with the theoretical search for new solutions and new numerical computational procedures, experimental methods for directly and indirectly measuring temperature and velocity are being developed.

While focusing on natural convection in a vertical channel [4,14,36], the case we have selected to achieve the aim of this work and to verify the solutions obtained in it, we realise that the problem is not clearly defined [5]. Depending on the width of the channel and the value of the Rayleigh number, different configurations of convective flow structures may occur in it, which also depend on the type of heating (symmetrical [6,19,41] or asymmetrical [2,3,23,43]), its surface temperature (constant or variable [37], or with a constant heat flux [1]), the presence or absence of side walls etc. Heat transfer in closed channels (horizontal, vertical or oblique) leads to the formation of Rayleigh–Bénard cells, which in open channels, especially wider ones, are blurred by the lateral flow of the medium into the channel.

In the context of this work, we must mention the new method of air temperature detection using thermovision [24,25] that we developed and used to study temperature fields in channels [26,27]. The results reported in the latter two papers inspired us to explore the possibility of reconstructing the velocity field on the basis of the temperature field detected by means of a thermal imaging camera. This includes situations when, for technical reasons, the velocity cannot be measured directly.

To date, experimental studies of free convection have concentrated more on determining the temperature field, from which the gradient method can be used to derive the heat flux on the heating wall. Velocity measurements have also been carried out, but here the focus is more on measuring the streamline, as this leads to a better understanding of the structure of convective flows. However, knowledge of the velocity field in convective flow is equally important, for example, because of the possibility of determining the flow resistance, which is dependent on the velocity gradient on the wall (shear stress), the non-Newtonian liquids used in the research, and the use of pump power in forced convection.

The above methods of detecting or modelling temperature fields are currently being used in conjunction with modern techniques for measuring velocity. The usual methods for detecting velocity fields are generally referred to as VBTP (Visualisation by Tracer Particles) and their combinations [22,33,39], in particular PIV (Particle Image Velocimetry) [12,16,18,38,40,42] and LDA (Laser Doppler Anemometry), with which small velocity vectors can be measured precisely in both air [9,10,28] and water [1]. These two methods have been combined, for example, in turbulence measurements in unsteady swirling [17]. One of the most interesting and thoroughly documented works, combining velocity field analysis with temperature fields, will be found in Betts and Bokhari [8], which deals with turbulent natural convection in a tall, enclosed cavity. On the basis of the experimental data given in this paper and others in the form of temperature and velocity distributions, calculations were carried out using the numerical reconstruction procedure (NRP) and the correctness of the results obtained for two velocity components was verified. The method that we have developed, the subject of this paper, is an extension and continuation of the research described in Ryms et al. [34], and focuses on the reconstruction of just one component of the velocity in free convective air flow around a double-sided heated vertical plate. The method developed in this work is correct for $\mathrm{Pr} \approx 1.0$, i.e. for air. For other liquids $\mathrm{Pr} \neq 1.0$, e.g. water, additional verification of the NRP method is required.

2. Experimental data processed by the NRP into velocity fields

2.1. Characteristics of convection cases used for verification

Two cases of convective heat transfer were selected to evaluate the correctness and accuracy of the proposed NRP based on the reconstruction of a velocity field from a knowledge of the temperature field. Both cases pertain to a vertical channel (gap) formed between two flat isothermal heat-transfer surfaces. In the first case, one of the surfaces is heated and the other is cooled, and the gap between them from the top, bottom and sides is surrounded by adiabatic surfaces [8]. This case was chosen by carrying out simultaneous measurements of the temperature and velocity distribution in the channel. As a result, the velocities reconstructed on the basis of the temperatures using the NRP can be compared with the actual velocities obtained for the same conditions. However, the authors of this work were aware of the fact that in Betts and Bokhari [8] the temperature and velocity fields were not given, only their distributions at nine different channel heights.

Therefore, for the experimental verification of the NRP, the possibility of using the test results of another case of convective heat transfer was also taken into account, i.e. in symmetrically heated vertical channels open on all sides [26,27]. The advantage of these results is that the distribution of temperature fields is obtained in the cross-section of the entire channel, not just at certain levels, whereas the disadvantage is that there are no velocity measurements. Although the results of the simultaneous measurement of temperature and velocity [1] were obtained for this case, they could not be used in this work, because the walls of the channel were not isothermal, only transmitting a constant heat flux; in addition, water was the medium in these tests, not air.

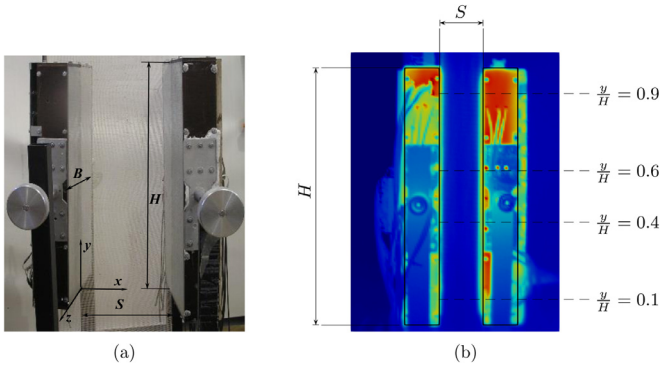

Fig. 1. The view of (a) a channel formed by two isothermal symmetrically heated vertical plates with a mesh between them, (b) the image from a thermal imaging camera along with the visualisation of temperature fields inside the channel obtained for the case $H = 500$ mm, $S = 85$ mm, $T_w = 323.15$ K, $T_\infty = 299.15$ K, $\Delta T = 24$ K, $\mathrm{Ra} = 2.53 \times 10^8$.

In this situation, it was decided to use the test results reported in Lewandowski et al. [26] and Lewandowski et al. [27], and the velocities calculated using the NRP were verified with SNC, as in Amine et al. [1].

2.2. Temperatures in an asymmetrically heated, closed channel

The first verification of the correctness of determining the velocity fields using the NRP was given by the results of free convection tests in an enclosed space [8] in the form of temperature distributions in an asymmetrically heated vertical channel of dimensions $H = 2.18$ m, $B = 0.52$ m and $S = 0.076$ m. Temperature distributions were studied experimentally using a 75 μm-diameter single traversed K-type Chromel–Alumel thermocouple. The velocity components u_y and u_x were measured using a single component LDA system with a 15 mW He-Ne laser in forward scatter mode with a dual Bragg shift and beam expander. As these methods are well known, there is no need to describe them in greater detail. The results in Betts and Bokhari [8] were tested for two cases of heat transfer in air, in which the temperature of the cold, water-thermostatted plate, was the same – $T_{cold} \approx 287$ K. The hot plate temperatures, on the other hand, were different: $T_{hot} \approx 307$ K ($\Delta T = 19.6$ K, $\mathrm{Ra} = 0.86 \times 10^6$) and $T_{hot} \approx 327$ K ($\Delta T = 39.9$ K, $\mathrm{Ra} = 1.43 \times 10^6$). Only the first case was used to verify the correctness of the calculations carried out with the NRP. The mean temperature and velocity variations within the cavity were found to be closely two-dimensional. The experimental results given in Betts and Bokhari [8] can be regarded as a benchmark for low turbulence Reynolds number flow.

2.3. Characteristics of the temperature field in a symmetrically heated open channel

To verify the correctness of the NRP, the matrix of the results of temperature distribution taken from Lewandowski et al. [26] and Lewandowski et al. [27] was used. Those papers examined free convection in open vertical gaps of width of $S = 0.045$, 0.085 and 0.15 m, formed between two isothermal and parallel heating plates of dimensions $H = 0.5$ m and $B = 0.25$ m and heating surface temperatures $T_w = 303$, 313, 323, 328, 333 and 343 K. The temperature field (Fig. 1) obtained for half the range of tested gaps and temperatures ($S = 0.085$ m, $T_w = 323$ K and $T_\infty = 299$ K) was selected from among the results given in those papers.

The results, obtained with an unusual method – a thermal imaging camera was used with a mesh as the air temperature detector – were considered reliable as this approach had been previously tested on a vertical plate [24] and also proved successful in determining heat losses in construction [25]. The test stand, in particular the heating plates used in it [35], was also checked to ensure it was operating properly.

3. Numerical approach

3.1. Background

The method first proposed in Ryms et al. [34] relies on conversion solely on the basis of the temperature field from a thermal imaging camera to a two-dimensional velocity field. This is possible because the Navier–Stokes, Fourier–Kirchhoff and continuity equations are coupled, so knowing the value of the temperature field is synonymous with knowing that of the velocity field in free convection problems. Moreover, this known temperature field in a fluid is caused by a difference in density, which in turn generates a fluid velocity field as a result of buoyancy. Since the variables are coupled, the fluid velocity can be determined from the temperature field. According to Ryms et al. [34], however, it has to be assumed that $u_x \approx 0$, which is true for the boundary layer assumption. This also means that the range of application is covered only in the region of developed flow on a vertical plate, i.e. in the region where the boundary layer forms. Otherwise, the simplifying condition $u_y \gg u_x$ is not fulfilled and the inconsistency of the solution obtained with the experiment data precludes its practical use. In view of the above limitations, we take a new approach to the reconstruction of the velocity field, i.e. the Numerical Reconstruction Procedure (NRP), in which the previous simplifications are not required.

3.2. Numerical reconstruction procedure (NRP)

The NRP makes it possible to use solely the temperature distribution from the thermal camera and hence obtain the velocity field by means of the numerical solution of the continuity equation

$$\nabla \cdot \mathbf{u} = 0 \tag{1}$$

together with a modified Navier–Stokes equation

$$\frac{\partial \mathbf{u}}{\partial t} + \nabla \cdot (\mathbf{u}\mathbf{u}) = \mathbf{S}_u - \nabla p_k + \nu \nabla \cdot \nabla \mathbf{u} \tag{2}$$

or Reynolds equation

$$\frac{\partial \bar{\mathbf{u}}}{\partial t} + \nabla \cdot (\bar{\mathbf{u}}\bar{\mathbf{u}}) = \bar{\mathbf{S}}_u - \nabla\left(\bar{p}_k + \frac{2}{3}k\right) + \nabla \cdot \left((\nu + \nu_t)\left(\nabla \bar{\mathbf{u}} + (\nabla \bar{\mathbf{u}})^{\mathrm{T}}\right)\right) \tag{3}$$

where $p_k = p\rho_0^{-1} - \mathbf{g} \cdot \mathbf{r}$ is the modified kinematic pressure, $\mathbf{g}$ is the gravity acceleration vector and $\mathbf{r}$ is the position vector. The eddy viscosity ν_t is modelled according to a given turbulence model, which in our case was identical to the SNC method ($k - \omega$ SST). The most important modification of the Navier–Stokes (2) or Reynolds (3) equation is the additional term $\mathbf{S}_u$ related to the source of the momentum, which has the same form of an additional term related to the Boussinesq approximation, namely

$$\mathbf{S}_u = -\beta(T - T_0)\mathbf{g} \tag{4}$$

where β is the coefficient of volumetric expansion and T_0 stands for the known reference temperature. In this way, the influence of temperature distribution T on the velocity field occurs through the momentum source term $\mathbf{S}_u$. It should be emphasised once again here that in the NRP there is no need to take into consideration an additional Fourier–Kirchhoff equation, nor do boundary conditions for temperature have to be specified. This is because we use temperature distributions from a thermal camera through the source of the momentum.

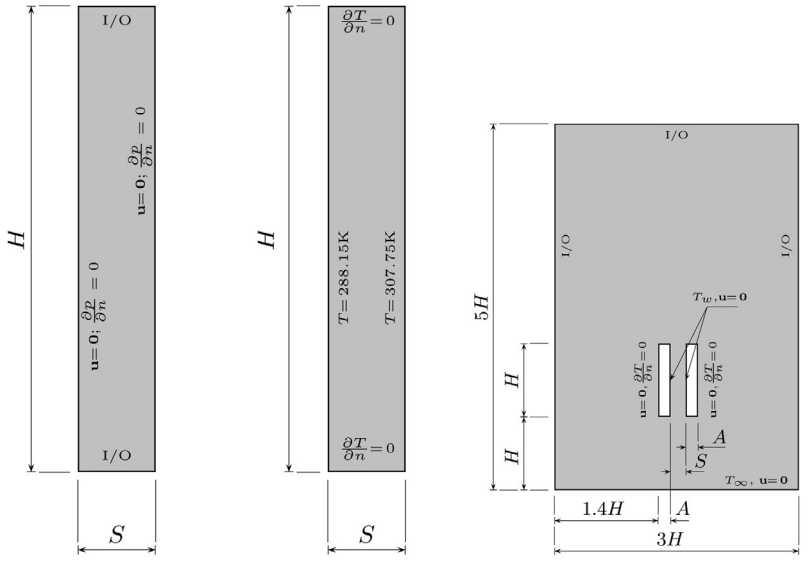

(a) Equally heated channel (NRP), $H = 500$ mm, $S = 85$ mm

(b) Differentially heated channel (SNC, NRP), $H = 2180$ mm, $S = 76$ mm [8]

(c) Equally heated channel (SNC), $H = 500$ mm, $S = 85$ mm, $A = 65$ mm, $T_w = 323.15$ K, $T_\infty = 299.15$ K

Fig. 2. SNC and NRP computational domains – dimensions and boundary conditions.

In order to implement the NRP, the existing software [32] was modified in such a way that the additional source term (4) was added to the centroid P of each finite volume V_P. For instance, the modified Navier–Stokes Eq. (2) is discretised by means of the finite volume method [21,30] resulting in

$$\frac{\mathrm{d}\mathbf{u}_P}{\mathrm{d}t}|V_P| + \sum_f \mathbf{u}_f \mathbf{u}_f \cdot \mathbf{S}_f = \mathbf{S}_u|V_P| - \sum_f p_{kf}\mathbf{S}_f + \nu \sum_f (\nabla \mathbf{u})_f \cdot \mathbf{S}_f \tag{5}$$

The linearised momentum source term (4) is discretised fully explicitly, i.e. $\mathbf{S}_u|V_P|$. This is possible because the momentum source term (4) does not depend on $\mathbf{u}$. In the above equation, $|V_P|$ is the control volume measure around a centroid P, and f stands for the index number of planar surfaces S_f around the control volume V_P.

The discretised convection terms are interpolated by means of bounded and limited linear interpolation with a blending coefficient of 0.2. Furthermore, the discretised Laplacian terms involving surface normal gradients make use of orthogonal schemes. The gradients involve Gaussian integration and linear interpolation. Finally, the fluxes are also based on linear interpolation. The discretised governing equations can be solved using the SIMPLE [11] algorithm. The pressure equation is solved by means of the generalised geometric-algebraic multi-grid (GAMG) solver with the diagonal-based incomplete Cholesky (DIC) smoother, while smooth solvers with a Gauss–Seidel smoother are used for the velocity components. Finally, the under-relaxation factors are 0.3, 0.7 and 0.5 for the pressure, velocity and turbulent quantities respectively, if applicable, and the constant values of parameters adopted for the calculations are $\beta = 0.003\,\mathrm{K}^{-1}$ and $\nu = 1.627 \times 10^{-5}\,\mathrm{m}^2\,\mathrm{s}^{-1}$.

3.2.1. Equally heated channel

The size of the computational mesh corresponds with the channel between the heated plates as well as the camera resolution (320×240) and is 27×149. The computational domain dimensions are shown in Fig. 2(a). No-slip conditions are specified on the left and right heated walls of the channel accompanied by a zero-gradient condition for pressure. The so-called inlet/outlet (I/O) boundary conditions are specified on the upper and lower boundaries of the domain. This means that mixed-type velocity boundary conditions are applied, i.e. for the inflow the velocity is obtained from the face normal component of the internal-cell value and for the outflow a zero-gradient condition is applied. Furthermore, the modified pressure p_k is calculated by a specification of the total pressure. Finally, the reference temperature is $T_0 = 299.15$ K. The results and comparisons are discussed in Section 3.4.

3.2.2. Differentially heated channel

The temperature-related boundary conditions are shown in Fig. 2(b). The velocities on the walls correspond to the no-slip condition. Also, the pressure gradient is calculated such that the flux on the boundary follows the velocity boundary condition. A 20×100 computational mesh was adopted such that the smallest possible mesh gives good agreement with the experimental data [8] according to the SNC method, discussed further in Section 3.3. Afterwards, the velocity distribution was reconstructed solely from the temperature distribution, which consisted in solving the continuity equation, the modified Reynolds equation as well as the k and ω transport equations without the Fourier–Kirchhoff equation. The reference temperature is $T_0 = 293.15$ K. Results and comparisons are provided in Section 3.4.

It is important to note that such a system of equations with these boundary conditions but without modifying the Reynolds or Navier–Stokes equation would result in a trivial solution, i.e. a zero-velocity field, as the system of equations to be solved describes incompressible flow without buoyancy. Only on the basis of the modified Reynolds (Navier–Stokes) equation containing an additional temperature-dependent term (known by default from the thermal imaging camera) could the velocity field be reconstructed.

3.3. Standard numerical calculations (SNC) of the experiments

In order to compare the velocity field obtained using the NRP, standard numerical calculations (SNC) of the experiments were

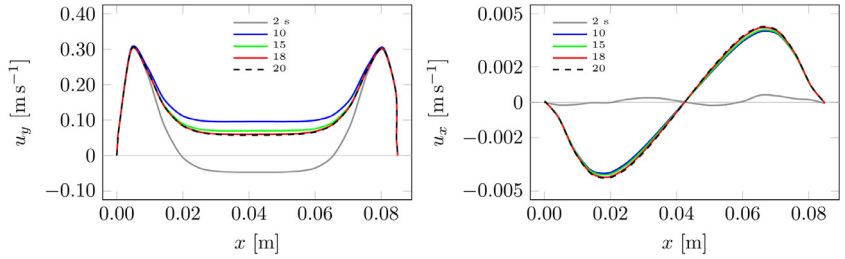

(a) u_y component (b) u_x component

Fig. 3. Equally heated channel – SNC temporal convergence, $y/H = 0.9$.

carried out in the domains with the dimensions shown in Fig. 2(c) and (b). An additional benefit of the SNC is that the temperature distributions could also be compared. Moreover, since the experimental data [8] were measured only at certain locations and the NRP required the distribution of temperatures in the centroid of each finite volume, the temperature distribution was determined using SNC. The resulting temperature distribution thus replaces the distribution known from the thermal imaging camera.

The most general set of governing equations was considered, i.e. the turbulent compressible flow, which does not take the Boussinesq approximation into account. This permits an additional evaluation of the proposed NRP of determining velocity fields based solely on temperature fields. Turbulence modelling involves a Reynolds Averaged Simulation with turbulence closure based on linear eddy viscosity supplemented with the two-equation $k-\omega$ SST [29] model. The choice of the turbulence model itself depends on the phenomenon and is preceded by some tests. In our case, the $k-\omega$ SST two-equation model gave very good compliance with the experimental data [8].

Finally, the constant values of other parameters adopted for both calculations are $c_p = 1004\,\mathrm{J\,kg^{-1}\,K^{-1}}$, $\mathrm{Pr} = 0.705$ and $\mu = 1.831 \times 10^{-5}\,\mathrm{kg\,m^{-1}\,s^{-1}}$. The turbulent quantities are set according to the low turbulence intensity and the turbulent Prandtl number is $\mathrm{Pr_t} = 0.85$. The $\mathrm{Pr_t}$ number is an empirical quantity and takes a constant value. There is a general consensus that $\mathrm{Pr_t}$ is of the order of 1. Generally, the values are in the range of 0.7–0.9 (e.g. [13]) with an average value 0.85, which works well in most cases. A scalable wall function is also applied to ensure stability.

3.3.1. Equally heated channel

The computational domain dimensions and boundary conditions are shown in Fig. 2(c). The no-slip conditions are specified on the bottom wall as well as on the heated walls together with the pressure gradient calculated such that the flux on the boundary follows the velocity boundary condition. The left, right and top walls are regarded as inlet/outlet (I/O) boundaries. Moreover, the size of the two-dimensional and Cartesian mesh adopted for the calculations was carefully chosen and consisted of 149 280 volumes. The maximum y^+ values are lower than those for the plate walls.

The transient system of governing equations is solved by means of the PISO algorithm [20], and the pressure equation is solved using the GAMG solver with the DIC Gauss–Seidel smoother. Preconditioned bi-conjugate gradient solvers using diagonal-based incomplete lower upper (DILU) preconditioners were utilised for the velocity fields, enthalpy and turbulent quantities. The total calculation time was 20 s with a time step ensuring that the Courant number $\mathrm{Co} < 1$. The temporal convergence is shown for different times and $y/H = 0.9$ in Fig. 3. From this figure it follows that from 18 s onwards, the u_y velocity component is stabilised, whereas the u_x component stabilises much earlier.

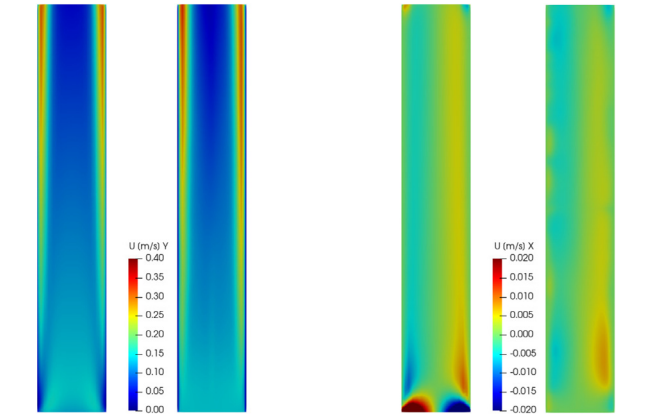

(a) u_y – SNC (left), NRP (right) (b) u_x – SNC (left), NRP (right)

Fig. 4. Equally heated channel velocity components: SNC vs. NRP.

3.3.2. Differentially heated channel

The no-slip conditions are specified everywhere and the pressure gradient is calculated such that the flux on the boundary follows the velocity boundary condition. The top and bottom walls are considered to be adiabatic whereas a fixed temperature 288.15 K is assumed on the left wall and 307.15 K on the right one. The maximum y^+ values are less than five for the plate walls.

The discretised governing equations are solved using the SIMPLE algorithm. The pressure equation is solved by means of the GAMG solver with the combined DIC and Gauss–Seidel smoother in which DIC smoothing is followed by Gauss–Seidel. Stabilised preconditioned bi-conjugate gradient solvers with the simplified DILU preconditioner are utilised for the velocity components, enthalpy and turbulence quantities. The under-relaxation factors are 0.7 for pressure turbulence quantities k and ω, and 0.3 for velocity and enthalpy.

3.4. Results

The velocity components from the NRP and SNC method for an equally heated channel are compared in Fig. 5: there is very good agreement for both velocity components. There are small differences for low y/H values due to inlet effects that coincide with the location of the I/O boundary conditions in the NRP. Moreover, Fig. 4 shows a graphical comparison of the individual velocity components. The influence of inlet effects is also visible, especially for the u_x components.

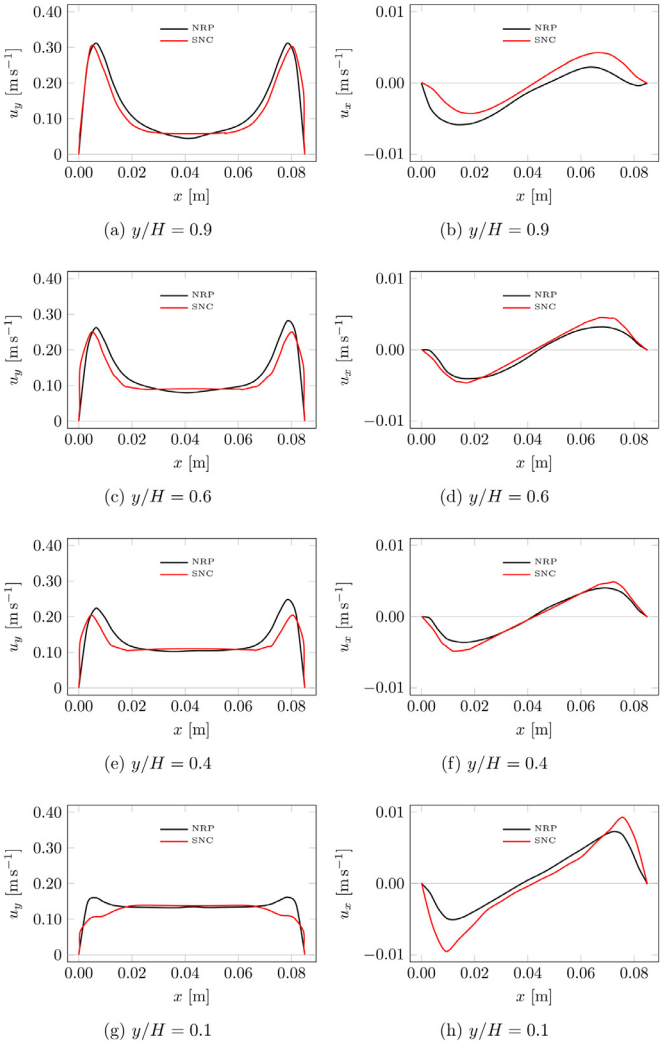

Fig. 5. Equally heated channel velocity distributions.

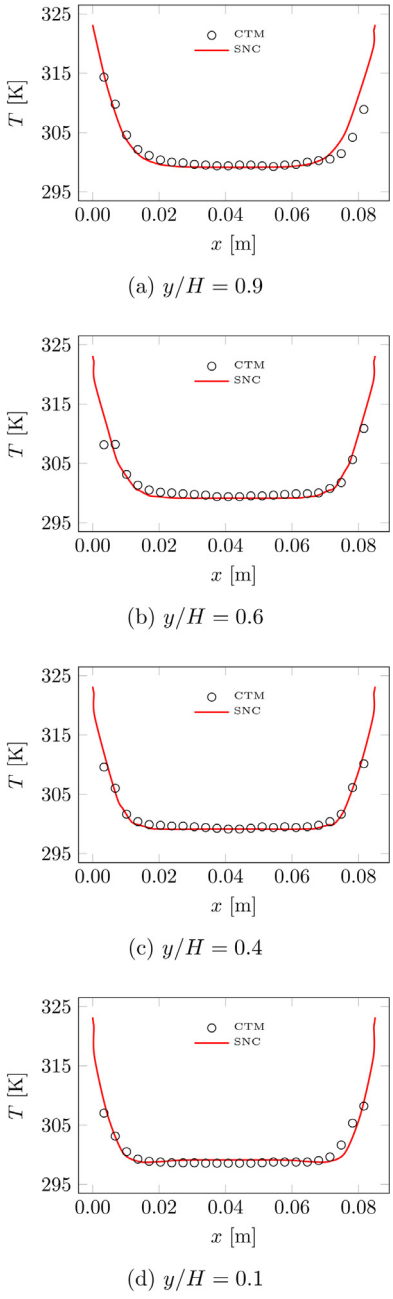

Fig. 6. Equally heated channel temperature distributions.

Fig. 6 compares the temperature distributions for SNC and CTM experimental data. The very good agreement of both methods indicates that the experiment was reliably reproduced numerically, which translates into a reliably solved velocity field.

The velocity components from the NRP and SNC method for a differentially heated channel are compared in Fig. 7. Again, the agreement is very good. This time, convection takes place in a closed cavity, which means that the boundary conditions can be unambiguously defined as no-slip walls. Consequently, there is no problem related to inlet effects. Again, one can see that the experiment was recreated correctly using the SNC method. This time, however, the temperature distributions from the SNC method replace the thermal camera data, on the basis of which the velocity components can be reconstructed. Furthermore, the selected velocity component measurements are also known from both the experiment and the SNC method. Importantly, the NRP and SNC method yield almost identical results, and both methods offer very good agreement with the experimental data.

4. Summary and conclusions

The novel method of reconstructing velocity fields (NRP) using experimental temperature measurements, outlined in this paper, can be applied to a variety of free convective heat transfer problems. Moreover, the NRP was positively verified directly from experimental results in a closed cavity with a differentially heated channel [8] and the results of standard numerical calculations (SNC) carried out for similar conditions in the vertical open channel in which experimental tests in the form of temperature fields are available [26,27]. However, the precondition for applying the NRP is a knowledge of the temperature field or the ability to measure it. Such cases occur, for example, in combustion chambers, heat exchangers, heat exchange in non-transparent media, narrow channels and channels, etc.

This new NRP method also creates new possibilities for thermal imaging cameras which, in addition to existing applications such as temperature measurements of surfaces and air, conducting energy audits, monitoring heat losses through thermal bridges and in medical diagnostics, will also be able (with appropriate software) to visualise air velocity fields, e.g. in free convective boundary layers, channels and cavities that are discussed in this paper.

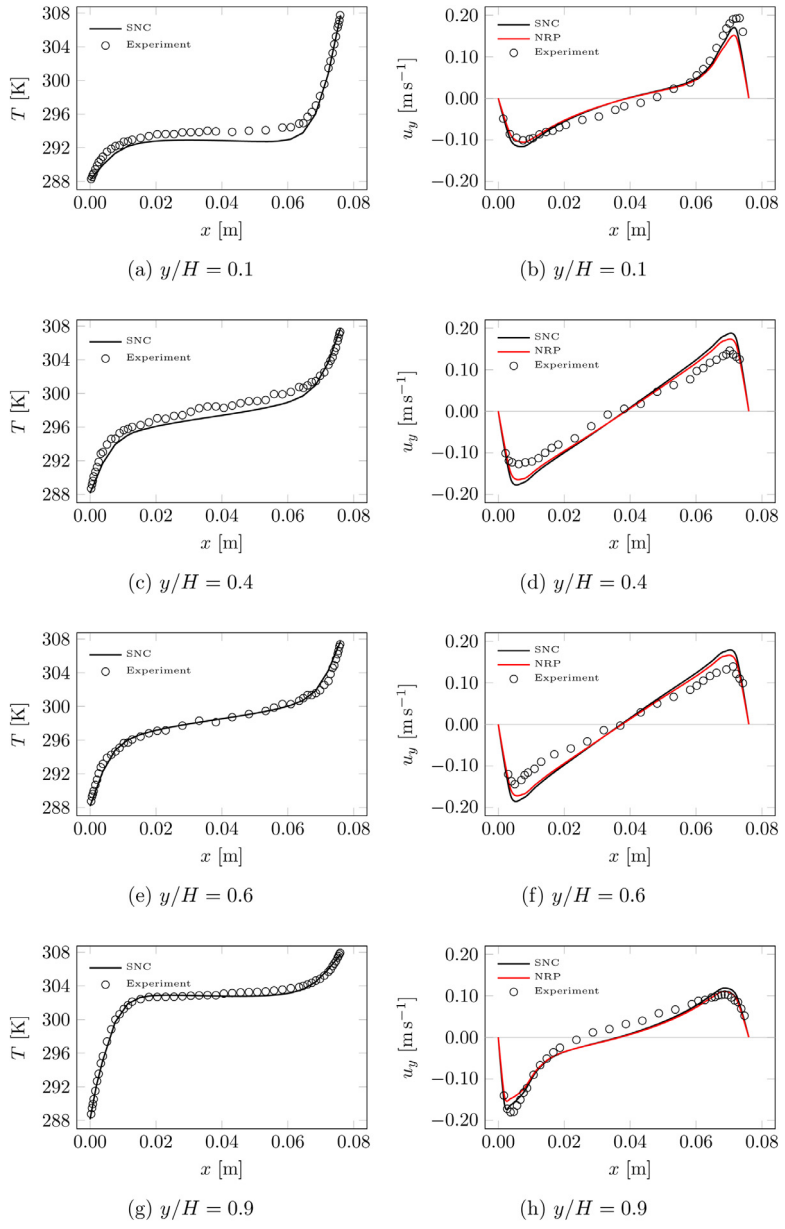

Fig. 7. Differentially heated channel: SNC vs. experiment [8] (left), SNC vs. NRP vs. experiment [8] (right).

The types of stationary flows that are suitable for reconstruction by NRP are in the range that can be recorded with a measuring mesh. Other types of flows such as plumes and jets are strongly three-dimensional and transient phenomena that are difficult to measure with a thermal camera and mesh. However, experimental and numerical studies on extending the applicability of the NRP are still in progress. Recreating non-stationary velocity fields requires recording and processing temperature fields at each time step.

The accuracy of the method depends on the resolution of the camera, as it corresponds directly with that of the computational mesh in the NRP. This is because the momentum source proportional to the temperature is added in the centroid of each finite volume. This also means that local temperature measurements cannot be used directly in the NRP unless these are interpolated/extrapolated on to the entire flow domain, i.e. on all centroids of the computational mesh. Moreover, since the thermal imaging camera with a temperature measurement accuracy of ≤ 0.1 K was used for recording the temperature field, we do not expect significant effect of uncertainty of these measurements on the accuracy of the NRP unless the measured temperature differences are lower than 1 K.

Declaration of Competing Interest

Authors declare that they have no conflict of interest.

CRediT authorship contribution statement

Krzysztof Tesch: Conceptualization, Data curation, Validation, Writing – original draft, Writing – review & editing. **Michał Ryms:** Conceptualization, Methodology, Data curation, Investigation, Writing – review & editing, Writing – original draft. **Witold M. Lewandowski:** Conceptualization, Writing – review & editing, Visualization, Validation, Supervision.

References

[1] Z. Amine, C. Daverat, S. Xin, S. Giroux-Julien, H. Pabiou, C. Ménézo, Natural convection in a vertical open-ended channel: comparison between experimental and numerical results, J. Energy Power Eng. 7 (2013) 1265–1276.

[2] A. Andreozzi, B. Buonomo, F. Cascetta, O. Manca, Transient air natural convection in asymmetrically heated vertical channels, Int. Commun. Heat Mass Transf. 116 (2020) 104697, doi:10.1016/j.icheatmasstransfer.2020.104697.

[3] W. Aung, Fully developed laminar free convection between vertical plates heated asymmetrically, Int. J. Heat Mass Transf. 15 (1972) 1577–1580, doi:10.1016/0017-9310(72)90012-9.

[4] A. Baïri, N. Laraqi, J.M.G. de María, Numerical and experimental study of natural convection in tilted parallelepipedic cavities for large Rayleigh numbers, Exp. Therm Fluid Sci. 31 (2007) 309–324, doi:10.1016/j.expthermflusci.2006.04.017.

[5] A. Baïri, E. Zarco-Pernia, J.M.G. de María, A review on natural convection in enclosures for engineering applications. The particular case of the parallelogrammic diode cavity, Appl. Therm. Eng. 63 (2014) 304–322, doi:10.1016/j.applthermaleng.2013.10.065.

[6] A. Bar-Cohen, W.M. Rohsenow, Thermally optimum spacing of vertical, natural convection cooled, parallel plates, ASME J. Heat Transf. 106 (1984) 116–123, doi:10.1115/1.3246622.

[7] B.R. Behera, V. Chandrakar, J.R. Senapati, Free convection heat transfer from a concave hemispherical surface: a numerical exercise, Int. Commun. Heat Mass Transf. 125 (2021) 105324, doi:10.1016/j.icheatmasstransfer.2021.105324.

[8] P.L. Betts, I.H. Bokhari, Experiments in turbulent natural convection in an enclosed tall cavity, Int. J. Heat Fluid Flow 21 (2000) 675–683, doi:10.1016/S0142-727X(00)00033-3.

[9] L.R. Cairnie, A.J. Harrison, Natural convection adjacent to a vertical isothermal hot plate with a high surface-to-ambient temperature difference, Int. J. Heat Mass Transf. 25 (1982) 925–934, doi:10.1016/0017-9310(82)90068-0.

[10] S. Caliskan, S. Baskaya, Velocity field and turbulence effects on heat transfer characteristics from surfaces with V-shaped ribs, Int. J. Heat Mass Transf. 55 (2012) 6260–6277, doi:10.1016/j.ijheatmasstransfer.2012.06.056.

[11] L.S. Caretto, A.D. Gosman, S.V. Patankar, D.B. Spalding, Two calculation procedures for steady, three-dimensional flows with recirculation, in: H. Cabannes, R. Temam (Eds.), Proceedings of the Third International Conference on Numerical Methods in Fluid Mechanics, Lecture Notes in Physics, 19, Springer, Berlin, Heidelberg, 1973.

[12] M.-S. Chae, B.J. Chung, Investigation of buoyancy influence on mixed convection in a vertical channel through PIV measurement, Int. J. Therm. Sci. 163 (2021) 106776, doi:10.1016/j.ijthermalsci.2020.106776.

[13] K.-A. Chang, E.A. Cowen, Turbulent Prandtl number in neutrally buoyant turbulent round jet, J. Eng. Mech. 128 (10) (2002), doi:10.1061/(ASCE)0733-9399(2002)128:10(1082).

[14] E.R.G. Eckert, W.O. Carlson, Natural convection in an air layer enclosed between two vertical plates with different temperatures, Int. J. Heat Mass Transf. 2 (1961) 106–120, doi:10.1016/0017-9310(61)90019-9.

[15] I.E. Ghandouri, A.E. Maakoul, S. Saadeddine, M. Meziane, Design and numerical investigations of natural convection heat transfer of a new rippling fin shape, Appl. Therm. Eng. 178 (2020) 115670, doi:10.1016/j.applthermaleng.2020.115670.

[16] S. Grafsronningen, A. Jensen, B.A.P. Reif, PIV investigation of buoyant plume from natural convection heat transfer above a horizontal heated cylinder, Int. J. Heat Mass Transf. 54 (2011) 4975–4987, doi:10.1016/j.ijheatmasstransfer.2011.07.011.

[17] N. Grosjean, L. Graftieaux, M. Michard, W. Hubner, C. Tropea, J. Volkert, Combining LDA and PIV for turbulence measurements in unsteady swirling, Meas. Sci. Technol. 8 (1997), doi:10.1088/0957-0233/8/12/015.

[18] Y. Hattori, T. Tsuji, Y. Nagano, N. Tanaka, Effects of free stream on turbulent combined-convection boundary layer along a vertical heated plate, Int. J. Heat Fluid Flow 22 (2001) 315–322, doi:10.1016/S0142-727X(01)00094-7.

[19] T. Inagaki, S. Maruyama, Turbulent heat transfer of natural convection between two vertical parallel plates, Heat Transfer-Asian Res. 31 (2002) 56–67, doi:10.1002/htj.10017.

[20] R.I. Issa, Solution of the implicitly discretized fluid flow equations by operator-splitting, J. Comput. Phys. 62 (1986) 40–65, doi:10.1016/0021-9991(86)90099-9.

[21] H. Jasak, Error Analysis and Estimation for the Finite Volume Method with Applications to Fluid Flows, 1996 Ph.D. thesis.

[22] D. Kim, D. Kim, M. Kim, J. Lee, I. Jung, K. Roh, K.C. Kim, Velocity field measurement on natural convection inside an automotive headlamp using time-resolved stereoscopic particle image velocimetry, Int. J. Heat Fluid Flow 77 (2019) 19–30, doi:10.1016/j.ijheatfluidflow.2019.03.004.

[23] K.M. Kim, D.H. Nguyen, G.H. Shim, D.-W. Jerng, H.S. Ahn, Experimental study of natural convection in open-ended vertical parallel plates under asymmetric heating conditions, Int. J. Heat Mass Transf. 159 (2020) 120135, doi:10.1016/j.ijheatmasstransfer.2020.120135.

[24] W.M. Lewandowski, M. Ryms, H. Denda, E. Klugmann-Radziemska, Possibility of thermal imaging use in studies of natural convection heat transfer on the example of an isothermal vertical plate, Int. J. Heat Mass Transf. 78 (2014) 1232–1242, doi:10.1016/j.ijheatmasstransfer.2014.07.024.

[25] W.M. Lewandowski, M. Ryms, H. Denda, Quantitative study of free convective heat losses from thermodynamic partitions using thermal imaging, Energy Build. 167 (2018) 370–383, doi:10.1016/j.enbuild.2017.12.047.

[26] W.M. Lewandowski, M. Ryms, H. Denda, Infrared techniques for natural convection investigations in channels between two vertical, parallel, isothermal and symmetrically heated plates, Int. J. Heat Mass Transf. 114 (2017) 958–969, doi:10.1016/j.ijheatmasstransfer.2017.06.120.

[27] W.M. Lewandowski, M. Ryms, H. Denda, Natural convection in symmetrically heated vertical channels, Int. J. Therm. Sci. 134 (2018) 530–540, doi:10.1016/j.ijthermalsci.2018.08.036.

[28] J.A. McWilliams, Review of Airflow Measurement Techniques, LBNL Report number, 2002.

[29] F.R. Menter, Two-equations eddy-viscosity turbulence models for engineering applications, AIAA J. 32 (8) (1994) 1598–1605, doi:10.2514/3.12149.

[30] F. Moukalled, L. Mangani, M. Darwish, The Finite Volume Method in Computational Fluid Dynamics, Springer, 2016.

[31] M. Ouakarrouch, K.E. Azhary, N. Laaroussi, M. Garoum, A. Feiz, Three-dimensional numerical simulation of conduction, natural convection, and radiation through alveolar building walls, Case Stud. Constr. Mater. 11 (2019) e00249, doi:10.1016/j.cscm.2019.e00249.

[32] OpenFOAM, https://www.openfoam.com.

[33] H. Park, J. Park, S.Y. Jung, Measurements of velocity and temperature fields in natural convective flows, Int. J. Heat Mass Transf. 139 (2019) 293–302, doi:10.1016/j.ijheatmasstransfer.2019.05.022.

[34] M. Ryms, K. Tesch, W.M. Lewandowski, The use of thermal imaging camera to estimate velocity proiles based on temperature distribution in a free convection boundary layer, Int. J. Heat Mass Transf. 165 (2021) 120686, doi:10.1016/j.ijheatmasstransfer.2020.120686.

[35] M. Ryms, W.M. Lewandowski, Evaluating the influence of radiative heat flux on convective heat transfer from a vertical plate in air using an improved heating plate, Int. J. Heat Mass Transf. 173 (2021) 121232, doi:10.1016/j.ijheatmasstransfer.2021.121232.

[36] R. Taher, M.M. Ahmed, Z. Haddad, C. Abid, Poiseuille–Rayleigh–Bénard mixed convection flow in a channel: heat transfer and fluid flow patterns, Int. J. Heat Mass Transf. 180 (2021) 121745, doi:10.1016/j.ijheatmasstransfer.2021.121745.

[37] S. Taieb, L.A. Hatem, J. Balti, Natural convection in an asymmetrically heated vertical channel with an adiabatic auxiliary plate, Int. J. Therm. Sci. 74 (2013) 24–36, doi:10.1016/j.ijthermalsci.2013.06.010.

[38] R.S. Volkov, P.A. Strizhak, Research of temperature fields and convection velocities in evaporating water droplets using planar laser-induced fluorescence and particle image velocimetry, Exp. Therm. Fluid Sci. 97 (2018) 392–407, doi:10.1016/j.expthermflusci.2018.05.007.

[39] R.S. Volkov, P.A. Strizhak, Using planar laser induced fluorescence and micro particle image velocimetry to study the heating of a droplet with different tracers and schemes of attaching it on a holder, Int. J. Therm. Sci. 159 (2021) 106603, doi:10.1016/j.ijthermalsci.2020.106603.

[40] C.E. Willert, M. Gharib, Digital particle image velocimetry, Exp. Fluids 10 (1991) 181–193, doi:10.1007/BF00190388.

[41] R.A. Wirtz, R.J. Stutzman, Experiments on free convection between vertical plates with symmetric heating, J. Heat Transf. 104 (1982) 501–507, doi:10.1115/1.3245121.

[42] T. Xue, S. Zhang, Investigation on heat transfer characteristics of falling liquid film by planar laser-induced fluorescence, Int. J. Heat Mass Transf. 126 (2018) 715–724, doi:10.1016/j.ijheatmasstransfer.2018.05.039.

[43] T. Yilmaz, S.M. Fraser, Turbulent natural convection in a vertical parallel-plate channel with asymmetric heating, Int. J. Heat Mass Transf. 50 (2007) 2612–2623, doi:10.1016/j.ijheatmasstransfer.2006.11.027.